Microfluid Nanofluid (2015) 19:1259–1269
DOI 10.1007/s10404-015-1634-9

RESEARCH PAPER

Pneumatic siphon valving and switching in centrifugal microfluidics controlled by rotational frequency or rotational acceleration

S. Zehnle[1] · F. Schwemmer[2] · R. Bergmann[1] · F. von Stetten[1,2] · R. Zengerle[1,2,3] · N. Paust[1,2]

Received: 2 May 2015 / Accepted: 12 August 2015 / Published online: 31 October 2015

Abstract Air-pressure-mediated, pneumatic siphon valves employ temporary storage and subsequent release of pneumatic energy, exclusively controlled by rotation of the disk. Implementation is easy, and robust valves can be integrated in a monolithic way at minimum additional costs. However, so far, pneumatic siphon valving requires deceleration from high to low rotational frequencies. Valve opening is performed always when the rotation of the disk drops below a critical rotational frequency. To overcome this limitation, we introduce new concepts for pneumatic siphon valving which enable operation of the disk at any rotational frequency without unwanted bursts of the siphon valves. Thus, the design space for pneumatic siphon valves in centrifugal microfluidics is significantly extended. Three types of pneumatic siphon valves are presented with release control at (1) rotational frequencies between 25 and 48 Hz, (2) positive rotational accelerations between 1 and 22 Hz s^{-1}, and (3) negative rotational accelerations between 5 and 20 Hz s^{-1}. Finally, we combine two valve types to realize robust switching into two fluidic paths with flow rate ratios of 94/6 and 0/100.

Keywords Centrifugal microfluidics · Valve · Switch · Pneumatic · Passive

1 Introduction

In the past decade, the field of centrifugal microfluidics has experienced a strong boost in research activity, which has resulted in continuous increase of scientific publications per year (Strohmeier et al. 2015). Low sample/reagent consumption and low costs per test, high portability and sensitivity, and short time-to-result are some of the potential advantages of microfluidic platforms in general (Mark et al. 2010). Centrifugal platforms in particular enable propulsion of liquids with a wide range of properties for scalable flow rates without the need for external pumps. Parallel processing in low-cost disposable plastic cartridges and no problems with gas bubbles are further aspects that make centrifugal microfluidics particularly attractive (Vázquez 2011). Applications of centrifugal microfluidics range from nucleic acid analysis through immunodiagnostics, clinical chemistry, and cell handling all the way to food and water analysis (Focke et al. 2010; Noroozi et al. 2011; Schembri et al. 1995; Burger et al. 2012; Garcia-Cordero et al. 2010; Hwang et al. 2013). Practically all of these applications require unit operations for the defined and precise handling of liquids. In particular, valving and switching steps are crucial in order to start and terminate certain process steps in a defined and controlled manner.

The valves that have been developed on centrifugal microfluidics platforms so far can be categorized into passive and active valves. While passive valves use the intrinsic centrifugation, only, in order to retain or release a certain amount of liquid, active valves employ external means such as heating, cooling, radiation, or pressure sources to

Electronic supplementary material The online version of this article (doi:10.1007/s10404-015-1634-9) contains supplementary material, which is available to authorized users.

✉ S. Zehnle
Steffen.Zehnle@Hahn-Schickard.de

[1] Hahn-Schickard, Georges-Koehler-Allee 103, 79110 Freiburg, Germany

[2] Laboratory for MEMS Applications, IMTEK - Department of Microsystems Engineering, University of Freiburg, Georges-Koehler-Allee 103, 79110 Freiburg, Germany

[3] BIOSS, Centre for Biological Signalling Studies, University of Freiburg, 79110 Freiburg, Germany

control the valve (Abi-Samra et al. 2011; Amasia et al. 2012; Kazarine et al. 2012).

By nature, passive valves obviate the need for cost-intensive equipment and are thus favoured over active valves, provided that they fulfill the same function. Passive valves can be further subcategorized into siphon valves and non-siphon valves. Non-siphon valves are for example capillary burst valves which use the capillary pressure that is induced when a meniscus pins at a sharp edge and counteracts the centrifugal pressure. In this way, the liquid is released when a certain critical rotational frequency is exceeded (Cho et al. 2007; Chen et al. 2008). A sharp pinning edge is not needed when hydrophobic coating is applied that raises the contact angle to more than 90° (Ouyang et al. 2013).

Mark et al. presented valving, metering, and aliquoting into dead-end chambers. A liquid volume is split into several metering fingers, each connected to a dead-end chamber. Due to air entrapment and resulting pneumatic counter pressure in the dead-end chamber, the liquid is retained at low centrifugation and released into the dead-end chamber at high centrifugation (Mark et al. 2009, 2011). Other passive non-siphon valves make use of assistive means such as additional liquids, burstable seals, dissolvable films, or membranes, capillaries and paper strips that are integrated into the centrifugal cartridge. Such assistive means require additional fabrication steps and may eventually increase complexity and costs (Kong et al. 2012; Ukita et al. 2012; van Oordt et al. 2013; Gorkin et al. 2012a; Hwang et al. 2011; LaCroix-Fralish et al. 2009; Kinahan et al. 2014).

Siphon valves are passive valves that use a bent fluidic channel with its crest at a radial innermost position. They connect a radial inner reservoir with a radial outer collection chamber and need to be primed by liquid up to a critical fill level in order to trigger the valving process and to transfer the liquid from the reservoir to the collection chamber by the centrifugal force, as depicted in Fig. 1.

Siphon priming has been realized in different ways: For contact angles less than 90°, the siphon can be primed by capillary action at low centrifugation, whereas the liquid is retained in the reservoir at high centrifugation (Schembri et al. 1995; Siegrist et al. 2010; Lutz et al. 2010; Steigert et al. 2007). Another way to prime a siphon is to induce Euler forces by applying high rotational acceleration. These Euler forces transfer a certain amount of liquid into a siphon. However, even with high acceleration rates (50 Hz s^{-1}) only small radial height differences (~2 mm) can be surmounted (Deng et al. 2014). Further methods of siphon priming employ additional liquids either to fill up the radial inner reservoir until the liquid level surpasses the siphon crest or to locally create a vacuum that drives the sample liquid into the siphon (Gorkin et al. 2012b).

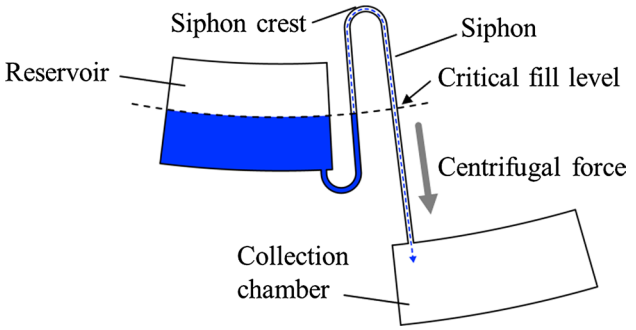

Fig. 1 Basic principle of siphon valving in centrifugal microfluidics. In closed state the liquid is retained in the radial inner reservoir, in open state the siphon is primed. Once the critical fill level for siphon priming is reached, the liquid is transferred from the reservoir into the collection chamber

Gorkin et al. (2010) used pneumatic action in order to prime a siphon during deceleration from high to low rotational frequencies. At high frequency, a sample liquid is pumped from a vented inlet chamber through a connecting inlet channel into an unvented pneumatic chamber and partially into a connected siphon. The air in the pneumatic chamber is entrapped and compressed by the incoming liquid. At high rotational frequencies, the compression is maintained and the liquid is kept in the pneumatic chamber. At lower frequencies, the compressed air volume expands and pushes the liquid back into the inlet channel but also into the siphon, which results in a higher fill level. Below a critical rotational frequency, the liquid is displaced so that it surpasses the siphon crest and the critical fill level for siphon priming, i.e., the valve opens. Major advantages of such a pneumatic siphon valve are a low dependence on wetting properties while obviating the need for external means or assistive materials. Due to its functioning as rotational frequency-triggered valve and due to its implementation as compression valve, we refer to it as rotational frequency-triggered compression valve (RFT-CV).

Recently, pneumatic siphon valving was presented with two pneumatic chambers that are connected via a narrow timing channel. This timing channel is used to control the speed of pneumatic energy release that in turn decides over siphon priming (Schwemmer et al. 2015; Zhao et al. 2015).

In this work we present three new types of pneumatic siphon valves, all based on four fluidic elements, namely a vented chamber, a pneumatic chamber, a siphon, and a flow resistor channel. In dependency on the arrangement of these fluidic elements, the individual siphon valves are triggered either by rotational frequency or by rotational acceleration, and they are implemented either as compression or as vacuum valves. Consequently, we refer to them as

1. Rotational frequency-triggered vacuum valve (RFT-VV)
2. Rotational acceleration-triggered vacuum valve (RAT-VV)
3. Rotational acceleration-triggered compression valve (RAT-CV)

Figure 2 shows the prior art RFT-CV and the three new valves classified according to their release control parameters rotational frequency (f) and rotational acceleration ($\mathrm{d}f/\mathrm{d}t$). The new valves presented in this paper are underlined.

As illustrated in Fig. 2 the parameter space spanned by f and $\mathrm{d}f/\mathrm{d}t$ can be divided into four regions representing four different classes of valves. A first class of valves is opened at low f, independent of $\mathrm{d}f/\mathrm{d}t$ (RFT-CV), a second class is opened at high f, independent of $\mathrm{d}f/\mathrm{d}t$ (RFT-VV), a third class is opened at high positive $\mathrm{d}f/\mathrm{d}t$ (RAT-VV) and a fourth class is opened at high negative $\mathrm{d}f/\mathrm{d}t$ (RAT-CV). The regions for the third and fourth classes of valves are indicated by shading. These valves are opened by fast change of the rotational frequency.

This paper is structured starting with a brief description of the simulation tool and the fabrication process that are used to design and manufacture the valves. Subsequently, the three new valves are introduced each with its functional principle and experimental results for proof of principle. Eventually, a combination of the RFT-CV and the RAT-CV is presented to build a switch that directs liquid through a first outlet siphon or through a second outlet siphon, dependent on the negative rotational acceleration (=deceleration) rate.

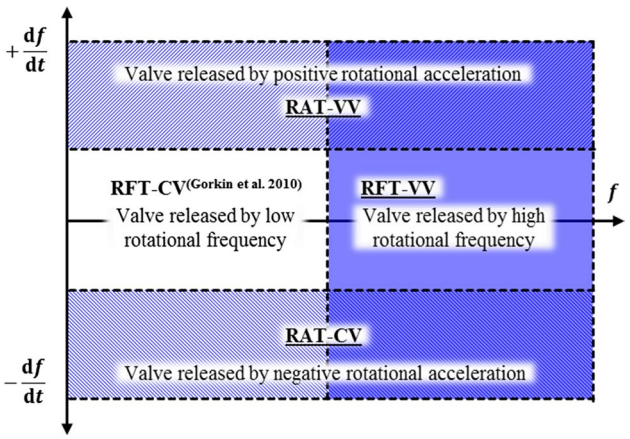

Fig. 2 Pneumatic siphon valves operated without assistive means, classified according to their control parameters rotational frequency (f) and rotational acceleration ($\mathrm{d}f/\mathrm{d}t$). The *marked fields* indicate the range of rotational parameters within which the different types of valves can be released. The new valves presented in this work are *underlined*

2 Materials and methods

In order to predict the performance of the valves, the microfluidic structures are translated into hydrodynamic networks with discrete elements. This lumped model approach has been presented in previous work (Zehnle et al. 2012a). In brief, discrete elements are models for channels with radial or isoradial orientation, chambers, ideal gas, and air vents. Each element represents a transfer function to relate the volumetric flow rate q through the element with the differential pressure Δp across the element. The total differential pressure across a fluidic element is the sum of the centrifugal pressure (Δp_c), the pneumatic pressure (Δp_p), the viscous pressure loss (Δp_v), the capillary pressure (Δp_{cap}), the Euler pressure (Δp_E), and the inertial pressure (Δp_i). In addition, models for fluidic capacitances caused by the bending of the sealing foil due to pressure changes are implemented. When the pressure in a fluidic chamber rises, the sealing foil bends outwards. Accordingly, under vacuum, the sealing foil bends into the chamber. Bending characteristics strongly depend on the shape of the sealed chamber and are determined empirically.

By integration of the volumetric flow rates, the liquid volume in each element is obtained and translated into fill levels to determine the position of liquid–air interfaces. Saber 2004.06 (Synopsys, CA, USA) simulation software is used to build up the fluidic network and to solve the flow equations numerically. Details of the fluidic network for each valve are presented in the Online Resource 1.

All valves presented in this paper are implemented in the LabDisk platform. They are designed in SolidWorks 2014 (Dassault Systèmes S.A., France) and realized in 4- to 6-mm-thick PMMA disks (Maertin & Co. AG, Germany) with a diameter of 130 mm, manufactured by micromilling using a KERN Evo (KERN Microtechnik GmbH, Germany) at Hahn-Schickard Lab-on-a-Chip Design + Foundry Service, Freiburg, Germany. After cleaning of the structured PMMA disks with DI-water and drying with pressurized nitrogen, they are sealed with a pressure-sensitive adhesive foil (#900320, HJ Bioanalytik, Germany) using lamination roles.

For experimental validation, each LabDisk is mounted on a spinning motor that is controlled via a personal computer with custom-made software that executes a predefined rotational protocol. Recording of real-time images is done with a stroboscopic light source and a camera. Both are synchronized with a motor to grab one image per revolution. A detailed description of the setup is given in the literature (Grumann et al. 2005). The recorded real-time images are used for evaluation of fill levels. These measured fill levels are used in the computer-aided design (CAD) in order to determine the corresponding volume. In this way, liquid volumes collected in chambers as well as

liquid volumes remaining in channels are determined by measuring the positions of the menisci.

3 Rotational frequency-triggered vacuum valve (RFT-VV)

The RFT-VV is a high-pass valve with respect to rotational frequency. This means that a certain critical rotational frequency f_{burst} of the LabDisk needs to be exceeded in order to prime the siphon and to transfer the liquid from the inlet chamber to the collection chamber as schematically depicted in Fig. 3.

A sample liquid is introduced into the inlet chamber through an inlet hole that is subsequently closed. Upon centrifugation, a fraction of the liquid is pumped out of the inlet chamber and partially fills the vented chamber and the siphon. In Fig. 3 the fill levels in the siphon are indicated by arrows. At the same time, the enclosed air in the inlet chamber is stretched by the volume of the liquid in the vented chamber, the flow resistor channel and the siphon. Hence, the inlet chamber acts as a pneumatic chamber with vacuum, i.e., air pressure below ambient pressure. At constant rotational frequency, the fill levels reach equilibrium: The centrifugal pressure exerted by the liquid column between r_1 and the liquid level in the vented chamber r_2 balances the pneumatic pressure in the inlet chamber.

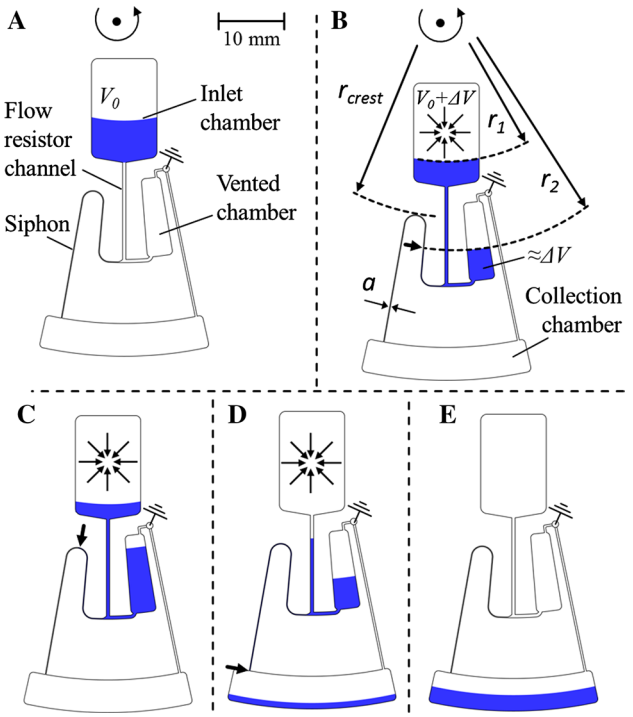

Fig. 3 Functional principle of the rotational frequency-triggered vacuum valve (RFT-VV) at increasing rotational frequency from **A** to **E**. **A** The liquid is loaded into the inlet chamber (=pneumatic chamber) that is subsequently closed. **b** While the rotational frequency rises, the liquid is transferred from the inlet chamber into the vented chamber and into the siphon (fill level indicated by *arrow*). **C** At the burst frequency, the liquid level in the siphon reaches the siphon crest. **D** Above the burst frequency, the liquid is transferred into the collection chamber. **E** Collection of the sample liquid. *Ground symbols* mark the air vents (=atmospheric pressure). For this type of valve, the flow resistor channel is designed with a large cross section to allow for fast liquid exchange between the inlet chamber and the vented chamber

Higher rotational frequencies yield higher centrifugal pressures that drive more liquid from the inlet chamber into the vented chamber and the siphon. Due to capillary pressure, the liquid level in siphon can slightly differ from the liquid level in the vented chamber. At the burst frequency, the sample liquid reaches the siphon crest. Below the burst frequency, the liquid can reciprocate between the pneumatic chamber and the vented chamber by increasing and decreasing the rotational frequency. Above the burst frequency, liquid is pumped into the descending part of the siphon and generates a centrifugal pressure that drives the liquid from the vented chamber and the pneumatic chamber into the collection chamber.

The burst frequency is calculated from the balance of the pneumatic pressure, the counteracting centrifugal pressure and the capillary pressure. Hence, it yields

$$f_{\text{burst}} = \frac{1}{2\pi}\sqrt{2\left(\beta p_0\left(1-\frac{V_0}{V_0+\Delta V(r_{\text{crest}})}\right)-\frac{4\sigma\cos(\theta)}{a}\right)\Big/\,\rho\left(r_{\text{crest}}^2-r_1(r_{\text{crest}})^2\right)} \quad (1)$$

where p_0 is the ambient air pressure, V_0 is the initial air volume in the inlet chamber at p_0, ΔV is the volume by which the air in the inlet chamber is stretched and can be approximated by the liquid volume in the vented chamber, ρ is the liquid density and β ($0 < \beta \leq 1$) is the empiric correction factor that accounts for bending of the sealing foil. The siphon width and depth are given by a, while σ is the surface tension of the liquid and θ is the contact angle. r_1 and r_{crest} are the radial positions of the liquid menisci at burst according to Fig. 3B, C. Both, r_1 and ΔV are functions of r_{crest}. Due to this dependency, the radial position of the siphon crest and chamber design can be used to tune the burst frequency. For the underlying valve implementation, $r_1(r_{\text{crest}})$ and $\Delta V(r_{\text{crest}})$ are given in the Online Resource 1 together with all numerical values.

4 RFT-VV: experimental results

For proof of principle of the RFT-VV, a disk with six valves is designed and fabricated. All six valves are identical except of the siphon height that varies with $r_{\text{crest}} = 35$–40 mm. All chambers are 3.5 mm deep, so that the volumes of the inlet chamber and the vented chamber amount to 541 and 142 µl, respectively. Channel cross

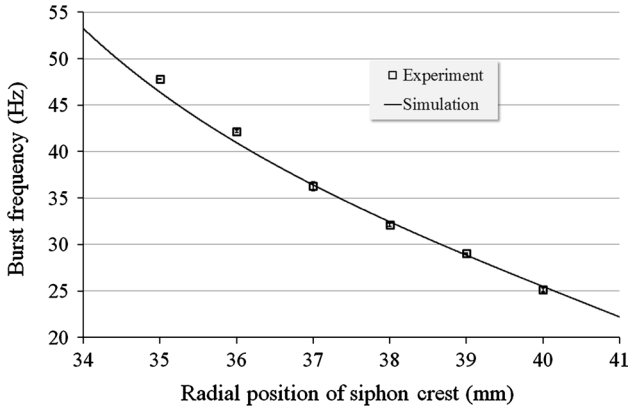

Fig. 4 Plot of the burst frequency of the RFT-VV against the radial position of the siphon crest r_{crest} for 200 µl of DI-water. *Error bars* indicate one standard deviation of the experimental results. The largest standard deviation is 0.5 Hz. All others standard deviations are smaller, thus the *error bars* are hardly visible

sections are chosen to 500 × 500 µm^2 for the flow resistor channel and 120 × 120 µm^2 for the siphon. According to Eq. 1, for this valve the burst frequency is independent of the cross section of the flow resistor channel. Hence, it is chosen large enough to not delay the liquid flow between the inlet chamber and the vented chamber. In the experiments 200 µl of DI-water are loaded into the inlet chamber which is then closed with a tape. In order to determine the burst frequencies for the different siphon heights, the rotational frequency is increased from 0 to 60 Hz with a ramp of 0.05 Hz s^{-1}. All experiments are carried out in triplicates.

Figure 4 shows the burst frequency plotted against r_{crest}. It confirms the decrease of burst frequency as the siphon crest moves radially outwards. Furthermore, the results of the network simulation and the experiments show good agreement, and the narrow error bars indicate that multiple valves with distinct burst frequencies can be addressed precisely.

5 Rotational acceleration-triggered vacuum valve (RAT-VV)

The RAT-VV is a high-pass valve with respect to rotational acceleration. This means that a certain critical rotational acceleration df/dt_{burst} of the disk needs to be exceeded in order to transfer the liquid from the inlet chamber to the collection chamber.

As depicted in Fig. 5, the RAT-VV features the same fluidic elements as the RFT-VV. However, slight changes in the dimensioning lead to the result that it cannot be opened by purely exceeding a burst frequency f_{burst}, but instead by exceeding a burst acceleration df/dt_{burst}.

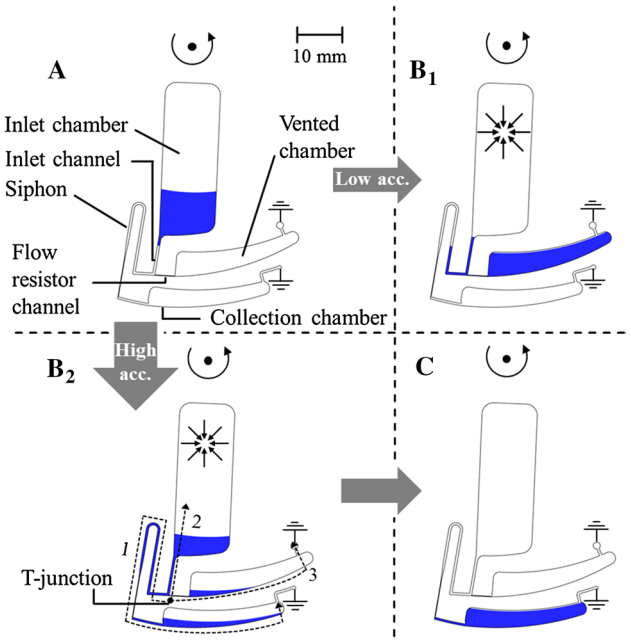

Fig. 5 Functional principle of the rotational acceleration-triggered vacuum valve (RAT-VV). **A** The liquid is pipetted into the inlet chamber (=pneumatic chamber) that is subsequently closed. **B$_1$** By applying slow acceleration, the liquid is transferred from the inlet chamber into the vented chamber and into the siphon without priming the siphon. **B$_2$** By applying fast acceleration, due to the high flow resistance of the flow resistor channel the siphon is primed and the liquid is transferred from the inlet chamber into the collection chamber. The *dashed arrows* indicate the pressure drops along the different fluidic paths 1–3 given by Eqs. 2, 3, 4. **C** Liquid collection

Similarly to the RFT-VV, the inlet chamber is loaded with the sample liquid and then closed. By applying a low rotational acceleration, the liquid is pumped from the inlet chamber into a vented chamber and into a siphon while generating a vacuum in the inlet chamber (Fig. 5A→B$_1$). This process is similar to the operation of the RFT-VV. The siphon crest of the RAT-VV, however, is located at a radial inner position that cannot be reached by the liquid as long as centrifugal pressure, the pneumatic pressure, and the capillary pressure are balanced. This is the case as long as the rotational acceleration df/dt is low, so that the volumetric flow rates q are low. The fluidic path between the inlet chamber and the vented chamber includes a section with a small channel diameter. This is the flow resistor channel that has a high hydraulic resistance. In case of high rotational acceleration of the disk, high flow rates are generated, and the flow resistor channel limits the flow into the vented chamber. As a consequence, the flow rate into the siphon is boosted so that the liquid level surpasses the siphon crest, and the liquid is pumped into the collection chamber (Fig. 5A→B$_2$).

It should be noted that priming of the siphon is driven by centrifugal force, which requires that the liquid level in

the inlet chamber remains higher than the siphon crest until the siphon is primed completely. This explains the necessity for increasing the rotational frequency fast enough to a high level before the liquid is drained off to the vented chamber.

A mathematical model of the RAT-VV can be obtained by defining three parallel fluidic paths. A first path defines the pressure drop Δp_1 from the T-junction along the siphon and the collection chamber to ground (=atmospheric pressure). A second path defines the pressure drop Δp_2 from the T-junction along the inlet channel to the inlet chamber, while a third path defines the pressure drop Δp_3 from the T-junction along the flow resistor channel and the vented chamber to ground. These pressure drops are composed by the different partial pressures (centrifugal, viscous, capillary, Euler, inertial, and pneumatic) in each path and read as follows

$$\Delta p_1 = \Delta p_{c1} + \Delta p_{v1} + \Delta p_{\mathrm{cap}1} + \Delta p_{E1} + \Delta p_{i1} \quad (2)$$

$$\Delta p_2 = \Delta p_{c2} + \Delta p_{v2} + \Delta p_{\mathrm{cap}2} + \Delta p_{E2} + \Delta p_{i2} + \Delta p_p \quad (3)$$

$$\Delta p_3 = \Delta p_{c3} + \Delta p_{v3} + \Delta p_{\mathrm{cap}3} + \Delta p_{E3} + \Delta p_{i3} \quad (4)$$

For detailed description of the single pressure terms the reader is referred to the Online Resource 1.

In order to apply Kirchhoff's law for closed loops, all fluidic paths are connected to a common ground whereby the pressure in the pneumatic chamber is linked to ground by the pneumatic pressure (last term of Eq. 3). Thus, we obtain

$$\Delta p_1(t) = \Delta p_2(t) = \Delta p_3(t) \quad (5)$$

and the flow rates at the T-junction node yield

$$q_1(t) + q_2(t) + q_3(t) = 0 \quad (6)$$

Siphon priming occurs if the liquid protrudes into the siphon far enough to generate a net centrifugal pressure in the radially descending siphon path that drives the liquid into the collection chamber. Hence, the liquid volume in the first path $V_{\mathrm{liq},1}$ must exceed a certain critical liquid volume V_{crit} such that the priming condition holds

$$V_{\mathrm{liq},1} = \int_0^\infty q_1(t)\,\mathrm{d}t > V_{\mathrm{crit}}. \quad (7)$$

The burst acceleration is a function of the spin protocol $f(t)$, of all channel and chamber dimensions and their positions, and of all fluid parameters. Such complex interdependencies cannot be solved in closed form. Thus, the burst acceleration is determined iteratively by numerical solution of the flow equations that describe the fluidic network for a given parameter set. For numerical solution of the flow equations, the network simulation approach is particularly suitable due to simple combination of lumped models. The network model along with an extension of Eq. 7 is provided in the Online Resource 1.

6 RAT-VV: experimental results

For proof of principle, RAT-VV type valves with four different cross-sectional areas of the flow resistor channel (100 × 100; 130 × 130; 145 × 145; 160 × 160 μm^2) are designed and fabricated. The cross section of the siphon is 500 × 500 μm^2. All chambers are 3.5 mm deep so that the volumes of the inlet chamber and the vented chamber amount to 1070 and 380 μl, respectively. Three hundred microliters of DI-water are loaded through an inlet hole in the inlet chamber which is then closed. Subsequently, the disk is spun with acceleration rates ranging between 0.25 and 24 Hz s^{-1} up to 50 Hz. Each run is carried out in triplicates and evaluated for siphon priming. Figure 6 shows the experimental results of the RAT-VV in comparison with the simulation. Both simulated and experimental results confirm that the valve remains closed for a certain lower range of rotational accelerations, i.e., process Fig. 5A→B$_1$ is executed, whereas the valve opens for a certain higher range of spin accelerations, i.e., process Fig. 5A→B$_2$ is executed. It can also be seen that the burst acceleration increases with the diameter of the flow resistor channel. This is because large channel cross sections of the flow resistor channel allow a larger fraction of the liquid to be pumped into the vented chamber during the period of acceleration. This fraction of liquid is not available in the inlet chamber to build up the centrifugal pressure that is needed to prime

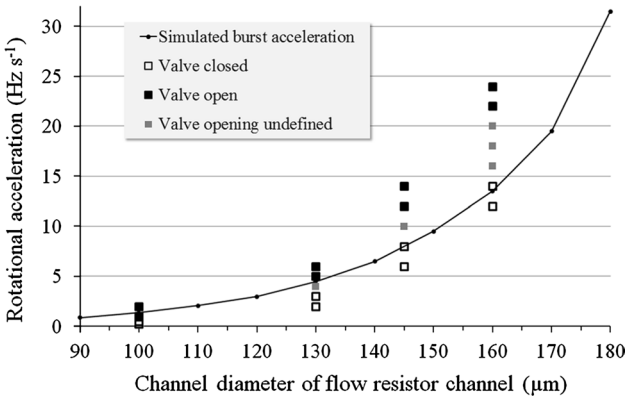

Fig. 6 Valve opening of the RAT-VV for varying channel diameters of the flow resistor channel. The burst acceleration rises as the diameter increases. *Filled squares* denote that the valves opened in each experiment. *Empty squares* denote that the valves remained closed in each experiment. *Gray squares* indicate that the valves opened only one or two times in three experiments. For the 100 × 100 μm^2 cross section, the valve remained closed at 0.25 and at 0.5 Hz s^{-1} and opened at 1 and 2 Hz s^{-1}

the siphon. Consequently, higher rotational frequencies are required to compensate for the liquid loss in the inlet chamber. Some parameter sets of the valve reveal a certain operating range in which valve triggering could not be performed reproducibly, i.e., siphon priming occurred in one or two times, only, out of three experiments. This may be due to variations in the bending of the sealing foil. Due to the large footprint of the pneumatic chamber, these variations are expected to be particularly high. Another reason could be variations of the capillary pressure due to fabrication tolerances and inhomogeneity of the surface roughness. In the narrow flow resistor channels, such variations lead to particularly strong changes of the capillary pressure.

7 Rotational acceleration-triggered compression valve (RAT-CV)

The RAT-CV is a high-pass valve with respect to negative rotational acceleration. This means that a certain critical deceleration df/dt_{burst} of the disk needs to be exceeded in order to transfer the sample liquid from the inlet chamber to the collection chamber. The process of RAT-CV valving is schematically depicted in Fig. 7 and can be regarded as an inversion of the RAT-VV valving: Here, the inlet chamber is vented and at high centrifugation liquid is pumped through the flow resistor channel into the unvented pneumatic chamber (Fig. 7B). In this type of valve, the enclosed air in the pneumatic chamber is compressed. At constant rotational speed, the pneumatic, centrifugal, and capillary pressures are balanced. Although the valve looks similar to the RFT-CV presented by Gorkin et al., it cannot be triggered by simply decreasing the rotational frequency to a certain critical value. Instead, the rate of deceleration is decisive.

By limiting frequency changes to a low deceleration rate, only low flow rates are induced and the liquid is pumped back into the vented inlet chamber with a minor fraction remaining in the ascending section of the siphon (Fig. 7C_1). This back-pumping without priming the siphon occurs because the fill levels in the siphon and in the inlet chamber rise equally. Slight deviations of the fill levels may be due to capillary force.

By applying high deceleration rates, the back flow of liquid into the inlet chamber occurs faster, and thus, a high flow rate is induced. This flow rate, however, is limited by the hydraulic resistance of the flow resistor channel. Therefore, more liquid flows into the siphon and primes the siphon completely (Fig. 7C_2). Subsequently, the entire liquid volume is transferred into the collection chamber (Fig. 7D).

A mathematical model of the RAT-CV is given by the same set of equations as for the RAT-VV (Eqs. 2, 3, 4). In order to account for the correct arrangement of the fluidic elements in comparison to the RAT-VV, the fluidic paths 2 and 3 are swapped as illustrated in Fig. 7C_2. Further details can be extracted from the Online Resource 1.

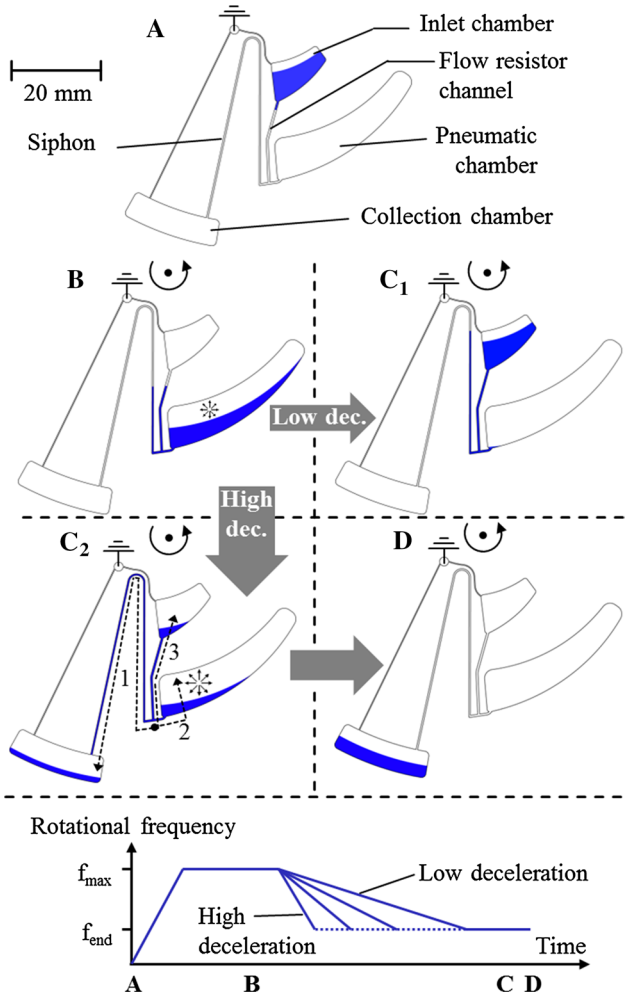

Fig. 7 Functional principle of the rotational acceleration-triggered compression valve (RAT-CV). **A** The liquid is loaded into a vented inlet chamber. **B** At high centrifugation, the liquid is pumped into the pneumatic chamber where the enclosed air volume is compressed. **C_1** By applying slow deceleration, the major part of the sample liquid is transferred back into the inlet chamber while the siphon is not primed. **C_2** By applying fast deceleration, the siphon is primed and the liquid is transferred into the collection chamber. The *dashed arrows* indicate the pressure drops along the different fluidic paths 1–3 given by Eqs. 2, 3, 4. **D** Liquid transfer completed

The resistance of the flow resistor channel determines the burst deceleration rate df/dt_{burst} above which the siphon is primed. A higher resistance leads to a lower df/dt_{burst} as the liquid is increasingly forced to flow into the siphon. Since only a small fraction of the liquid volume is required to prime the siphon, the resistance does not have to be particularly high. In fact, in this implementation, most of the

chosen cross sections of the flow resistor channel are equal or larger than the one of the siphon.

8 RAT-CV: experimental results

As for the RAT-VV type valve, the RAT-CV is characterized for four different cross-sectional areas of the flow resistor channel (300 × 300; 350 × 350; 400 × 400; 450 × 450 μm^2). The cross-sectional area of the siphon is chosen to 350 × 350 μm^2, while the pneumatic chamber is 2 mm deep and the vented chamber is 3.3 mm deep, so that their volumes amount to 502 and 267 μl, respectively. In each experimental run 150 μl of DI-water are loaded into the disk and centrifuged into the pneumatic chamber at $f_{max} = 50$ Hz. Subsequently, the rotational frequency is decreased at a specific deceleration rate to $f_{end} = 10$ Hz. By variation of the deceleration rate in different runs, the burst deceleration rate df/dt_{burst} is determined. All experiments are performed in triplicates.

Figure 8 shows the experimental results of the RAT-CV in comparison with the simulation. Both simulated and experimental results confirm that the valve remains closed for a certain lower range of rotational decelerations, i.e., process Fig. 7B→C_1 is executed, whereas the valve opens for a certain higher range of rotational decelerations, i.e., process Fig. 7B→C_2 is executed. It can also be seen that the burst deceleration increases with the diameter of the flow resistor channel. This is due to the effect that more liquid can escape through a broad flow resistor channel than through a narrow flow resistor channel during the period of deceleration. Hence, in case of using a broader flow resistor channel the pneumatic pressure is reduced faster. To compensate for this effect, the centrifugal counter pressure has to be lowered faster than the pneumatic pressure loss can take place.

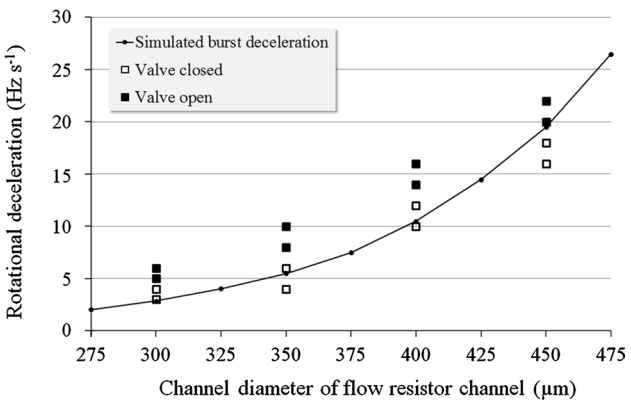

Fig. 8 Valve opening of the RAT-CV for varying channel diameters of the flow resistor channel. The burst deceleration rises as the diameter increases. *Filled squares* denote that the valves opened in each experiment. *Empty squares* denote that the valves remained closed in each experiment

The experimental results show good agreement with the simulation and a sharp transition from valve closure to valve opening. In order to show the particular robustness of the RAT-CV, additional parameter sets with different rotational protocols, a higher viscous liquid and a different liquid volume have been tested successfully. The results are given in the Online Resource 1.

For both acceleration-triggered valves (RAT-VV and RAT-CV) small variations of the flow resistor channel diameters result in significant changes in burst acceleration or deceleration. Larger variations of the channel diameters can be used to further tune the burst parameters, so that the number of valves with different burst accelerations or decelerations is limited only by the geometric boundary conditions given on the rotational platform, by the fabrication technology and by the rotational protocols that can be run. In addition, volumes, shapes, and positions of the vented and unvented chambers can be adapted to tune the burst parameters. In general, measures that result in an increased fill level in the siphon make siphon priming easier, i.e., reduce the burst acceleration or deceleration. Such measures are, e.g., increasing the entrapped gas volume in the vacuum valve and decreasing the entrapped gas volume in the compression valve, as well as making the chambers steeper such that higher liquid levels are reached for the same liquid volume contained.

9 Rotational acceleration-triggered compression switch (RAT-CS)

The potential of the hereby presented pneumatic siphon valves can be further developed to build passive switches for centrifugal microfluidics. As an example, we combine the prior art RFT-CV and the new RAT-CV to a rotational acceleration-triggered switch. Its functional principle is shown in Fig. 9. The switch is comprised of a vented chamber, an unvented pneumatic chamber, a flow resistor channel, a lower siphon 1 triggered by rotational frequency, and an upper siphon 2 triggered by rotational acceleration.

In operation, the switch works as follows. First, the liquid is loaded into a radial inner inlet chamber (Fig. 9A). Upon centrifugation, the liquid is pumped through the flow resistor channel into the pneumatic chamber where it encloses and compresses air. At constant rotational frequency, the liquid levels reach equilibrium where $\Delta p_c = \Delta p_p + \Delta p_{cap}$ (Fig. 9B). In Fig. 9 the fill levels are indicated by arrows. When the rotational frequency is decreased, the compressed air volume expands and displaces the liquid into both siphons and into the vented chamber.

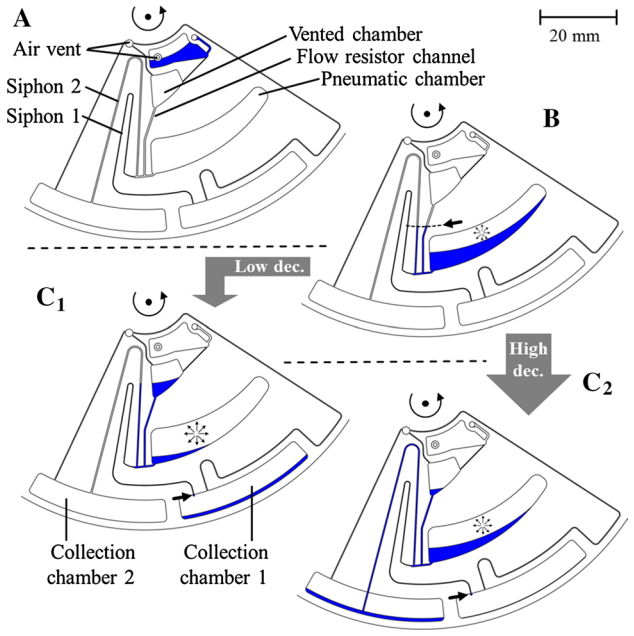

Fig. 9 Functional principle of the rotational acceleration-triggered compression switch (RAT-CS): A combination of the prior art RFT-CV and the new RAT-CV. **A** The liquid is loaded into an inlet chamber. **B** At elevated rotational frequency, the liquid is pumped radially outwards through the flow resistor channel into the pneumatic chamber where the air volume is enclosed and compressed (fill levels indicated by *dashed line* and *arrow*) $\mathbf{C_1}$ By applying slow deceleration, the liquid primes siphon 1, only. $\mathbf{C_2}$ By applying fast deceleration, the major part of the liquid is pumped through siphon 2

If this decrease in rotational frequency occurs at low deceleration rate, the liquid levels in the siphons and in the vented chamber rise with the same speed. This situation is similar to the one described in Fig. 7C_1 where only one siphon is used. Small variations of the fill levels may be due to capillary pressure. As soon as the rotational frequency drops below a certain critical value, the liquid levels in the vented chamber and in siphon 2 are higher than the crest of siphon 1. In this case siphon 1 is primed, only, such that the entire liquid volume is transferred into collection chamber 1 (Fig. 9C_1).

If the decrease in rotational frequency occurs at a high deceleration rate, the drop of centrifugal pressure is faster than the air volume in the pneumatic chamber can expand due to the limited flow through the flow resistor channel. In this case, more liquid is pumped through the siphons, and in particular, siphon 2 is primed, too. Since siphon 1 is designed with a much higher flow resistance than siphon 2, the liquid fraction that is collected in collection chamber 2 is significantly higher than the liquid fraction in collection chamber 1. We denote the transition between priming of siphon 1, only and priming of both siphons as critical deceleration rate.

As communicated in the literature, a challenge for the RFT-CV is premature priming of the siphon during initial loading of the pneumatic chamber (Gorkin et al. 2010; Godino et al. 2013; Zehnle et al. 2012b). A high hydraulic resistance of the flow resistor channel circumvents such premature priming but increases loading time and—more importantly—for the RAT-CS the critical deceleration rate would be decreased significantly. In order to reliably prevent premature priming of siphon 1 without the need for a high hydraulic resistance between vented and unvented chamber, the inlet structure is split into two chambers, the vented chamber and an auxiliary vented inlet chamber. Consequently, the flow of liquid during initial ramp-up is delayed, and it can be ensured that when a critical volume has entered the switch, the rotational frequency is sufficiently high to reliably prevent premature priming of siphon 1.

In analogy to the three valves (RFT-VV, RAT-VV, RAT-CV) presented in the previous chapters, the burst frequency of siphon 1 can be calculated from the balance of centrifugal pressure, pneumatic pressure and capillary pressure (cf. RFT-VV, Eq. 1), while priming of siphon 2 can be predicted by employing equation set 2–7. The network simulation setup that is used to solve for the flow equations is explained in the Online Resource 1.

10 RAT-CS: experimental results

The design of the RAT-CS is based on the design of the RAT-CV. Hence, a variation of the cross-sectional area of the flow resistor channel would affect the critical deceleration rate in a similar way as the burst deceleration rate of the RAT-CV shown in Fig. 8. For this reason, the RAT-CS is characterized for two different liquids that mainly differ in viscosity, namely DI-water ($\mu = 1$ mPa s) and a highly viscous lysis buffer ($\mu = 13$ mPa s). Into the disk, 150 µl of the liquids are introduced. For both liquids, a rotational protocol according to Fig. 7 with $f_{max} = 50$ Hz and $f_{end} = 15$ Hz is applied. For the lysis buffer, a period with $f = 40$ Hz is added to speed up the liquid transfer through siphon 1. All experiments are carried out in triplicates. In order to obtain reasonable critical deceleration rates for both liquids, the cross section of the flow resistor channel is tuned to 400 × 400 µm^2, while keeping the cross section of siphon 2 at 350 × 350 µm^2. The cross section of siphon 1 is set to 150 × 150 µm^2, with the first 3 mm of the siphon constricted to 100 × 100 µm^2 in order to increase the hydraulic resistance. Both the vented chamber and the pneumatic chamber are 2 mm deep, so that their volumes amount to 105 and 502 µl, respectively.

Figure 10 shows the experimental results in comparison with the simulation. Both, simulated and experimental

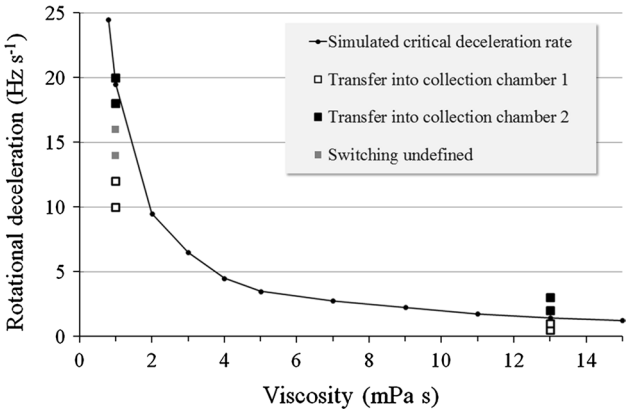

Fig. 10 Switching of the RAT-CS for varying viscosities. The critical deceleration rate marks the transition from liquid transfer into collection chamber 1 to liquid transfer into collection chamber 2, and it decreases as the viscosity increases. *Filled squares* mark the liquid transfer into collection chamber 2 in each experiment. *Empty squares* indicate no liquid transfer into collection chamber 2 in each experiment. *Gray squares* indicate that the transfer into collection chamber 2 occurred only one or two times in three experiments

results confirm that the liquid is transferred into collection chamber 1 for a certain lower range of rotational decelerations, i.e., process Fig. 9B→C_1 is executed, whereas for a certain higher range of rotational decelerations, the liquid is transferred into collection chamber 2, i.e., process Fig. 9B→C_2 is executed. Both also confirm that the critical deceleration rate decreases as the viscosity of the liquid increases. This is because rising viscosity has the same effect as constricting the flow resistor channel—both changes increase the hydraulic resistance of the flow resistor channel. In fact, the viscosity changes the hydraulic resistances in all paths of the fluidic network. Yet, since the large part of the liquid is pumped through the flow resistor channel, this path has the highest energy dissipation, thus is affected most by viscosity changes.

For the low deceleration rates, liquid transfer into collection chamber 1 could be performed with always less than 0.2 % liquid volume remaining in the fluidic network, while no liquid was transferred into collection chamber 2. For the high deceleration rates, the liquid transfer into collection chamber 2 is always accompanied with a certain loss into collection chamber 1. Evaluation of the liquid volumes collected yielded transfer efficiencies of 94 ± 2 % (simulation: 93 %) for water and 95 ± 1 % (simulation: 94 %) for the lysis buffer. Similar to the RAT-VV, a band of deceleration rates is identified, in which priming of siphon 2 is irreproducible, i.e., occurs in one or two out of three experiments, only. This is the case for 14–16 Hz s^{-1}. Again, this characteristic is attributed to variations in the bending of the sealing foil and to variations of the capillary pressure in the narrow siphon 1.

11 Conclusions

We presented three new types of pneumatic siphon valves that are all comprised of four basic design elements. A vented chamber is used as liquid storage chamber and is always at ambient pressure. An unvented chamber is exposed to pressure or vacuum that is well-defined by the spinning protocol and by the liquid volume in the system. A flow resistor channel limits the flow rate in order to delay equilibration of centrifugal and pneumatic pressures. A siphon enables liquid transfer to downstream elements after valving.

Dependent on the implementation of the four design elements, an RFT-VV-, RAT-VV- or an RAT-CV-type siphon valve is designed. Moreover, by combination of two siphon valves, the RAT-CS-type siphon switch is obtained.

All valve and switch performances were predicted with the network simulation. Experimental results showed good agreement and reliable operation for pre-defined operating conditions.

The concept presented in this work increases the number of operating parameters for passive valves in centrifugal microfluidics and leads to more freedom in the design of larger fluidic networks to build microfluidic process chains. Hence, it allows for implementation of complex workflows with purely passive valves.

The two vacuum valves (RFT-VV, RAT-VV) presented in this work are attractive for combination with liquid reagent pre-storage. In particular, the RAT-VV is designed such that stickpacks containing liquid reagents fit into the inlet chamber (van Oordt et al. 2013). While stickpack opening may be performed at high rotational frequency, the valving to downstream fluidics would be controlled by rotational acceleration.

The compression valve and the switch (RAT-CV, RAT-CS) presented in this work excel with large operating parameter spaces. In future work, the RAT-CV will be employed in sample-to-answer systems for nucleic acid analysis. Thanks to its two-way output, the RAT-CS enables reliable waste–eluate separation and can be employed for switching within workflows of immunoassays and DNA extractions.

Acknowledgments We gratefully acknowledge financial support by the Federal Ministry of Education and Research (BMBF) in the project EasyTube (Project Number 16SV5451K).

References

Abi-Samra K, Hanson R, Madou M, Gorkin RA (2011) Infrared controlled waxes for liquid handling and storage on a CD-microfluidic platform. Lab Chip 11(4):723–726. doi:10.1039/c0lc00160k

Amasia M, Cozzens M, Madou MJ (2012) Centrifugal microfluidic platform for rapid PCR amplification using integrated thermoelectric heating and ice-valving. Sens Actuators B Chem 161(1):1191–1197. doi:10.1016/j.snb.2011.11.080

Burger R, Kirby D, Glynn M, Nwankire C, O'Sullivan M, Siegrist J, Kinahan D, Aguirre G, Kijanka G, Gorkin RA, Ducrée J (2012) Centrifugal microfluidics for cell analysis. Curr Opin Chem Biol 16(3–4):409–414. doi:10.1016/j.cbpa.2012.06.002

Chen JM, Huang P, Lin M (2008) Analysis and experiment of capillary valves for microfluidics on a rotating disk. Microfluid Nanofluid 4(5):427–437. doi:10.1007/s10404-007-0196-x

Cho H, Kim H, Kang JY, Kim TS (2007) How the capillary burst microvalve works. J Colloid Interface Sci 306(2):379–385. doi:10.1016/j.jcis.2006.10.077

Deng Y, Fan J, Zhou S, Zhou T, Wu J, Li Y, Liu Z, Xuan M, Wu Y (2014) Euler force actuation mechanism for siphon valving in compact disk-like microfluidic chips. Biomicrofluidics 8(2):024101. doi:10.1063/1.4867241

Focke M, Stumpf F, Roth G, Zengerle R, von Stetten F (2010) Centrifugal microfluidic system for primary amplification and secondary real-time PCR. Lab Chip 10(23):3210–3212. doi:10.1039/c0lc00161a

Garcia-Cordero JL, Barrett LM, O'Kennedy R, Ricco AJ (2010) Microfluidic sedimentation cytometer for milk quality and bovine mastitis monitoring. Biomed Microdevices 12(6):1051–1059. doi:10.1007/s10544-010-9459-5

Godino N, Gorkin R, Linares AV, Burger R, Ducrée J (2013) Comprehensive integration of homogeneous bioassays via centrifugo-pneumatic cascading. Lab Chip 13(4):685–694. doi:10.1039/c2lc40722a

Gorkin R, Clime L, Madou M, Kido H (2010) Pneumatic pumping in centrifugal microfluidic platforms. Microfluid Nanofluid 9(2–3):541–549. doi:10.1007/s10404-010-0571-x

Gorkin R, Nwankire CE, Gaughran J, Zhang X, Donohoe GG, Rook M, O'Kennedy R, Ducrée J (2012a) Centrifugo-pneumatic valving utilizing dissolvable films. Lab Chip 12(16):2894–2902. doi:10.1039/c2lc20973j

Gorkin R, Soroori S, Southard W, Clime L, Veres T, Kido H, Kulinsky L, Madou M (2012b) Suction-enhanced siphon valves for centrifugal microfluidic platforms. Microfluid Nanofluid 12(1–4):345–354. doi:10.1007/s10404-011-0878-2

Grumann M, Brenner T, Beer C, Zengerle R, Ducrée J (2005) Visualization of flow patterning in high-speed centrifugal microfluidics. Rev Sci Instrum 76:025101

Hwang H, Kim H, Cho Y (2011) Elastomeric membrane valves in a disc. Lab Chip 11(8):1434–1436. doi:10.1039/c0lc00658k

Hwang H, Kim Y, Cho J, Lee J, Choi M, Cho Y (2013) Lab-on-a-disc for simultaneous determination of nutrients in water. Anal Chem 85(5):2954–2960. doi:10.1021/ac3036734

Kazarine A, Kong Matthew C R, Templeton EJ, Salin ED (2012) Automated liquid-liquid extraction by pneumatic recirculation on a centrifugal microfluidic platform. Anal Chem 84(16):6939–6943. doi:10.1021/ac301421k

Kinahan DJ, Kearney SM, Dimov N, Glynn MT, Ducrée J (2014) Event-triggered logical flow control for comprehensive process integration of multi-step assays on centrifugal microfluidic platforms. Lab Chip 14(13):2249–2258. doi:10.1039/c4lc00380b

Kong MCR, Bouchard AP, Salin ED (2012) Displacement pumping of liquids radially inward on centrifugal microfluidic platforms in motion. Micromachines 3(4):1–9. doi:10.3390/mi3010001

LaCroix-Fralish A, Templeton EJ, Salin ED, Skinner CD (2009) A rapid prototyping technique for valves and filters in centrifugal microfluidic devices. Lab Chip 9(21):3151–3154. doi:10.1039/b908683h

Lutz S, Weber P, Focke M, Faltin B, Hoffmann J, Müller C, Mark D, Roth G, Munday P, Armes N, Piepenburg O, Zengerle R, von Stetten F (2010) Microfluidic lab-on-a-foil for nucleic acid analysis based on isothermal recombinase polymerase amplification (RPA). Lab Chip 10(7):887–893. doi:10.1039/b921140c

Mark D, Metz T, Haeberle S, Lutz S, Ducrée J, Zengerle R, von Stetten F (2009) Centrifugo-pneumatic valve for metering of highly wetting liquids on centrifugal microfluidic platforms. Lab Chip 9(24):3599–3603. doi:10.1039/b914415c

Mark D, Haeberle S, Roth G, von Stetten F, Zengerle R (2010) Microfluidic lab-on-a-chip platforms: requirements, characteristics and applications. Chem Soc Rev 39(3):1153–1182. doi:10.1039/b820557b

Mark D, Weber P, Lutz S, Focke M, Zengerle R, von Stetten F (2011) Aliquoting on the centrifugal microfluidic platform based on centrifugo-pneumatic valves. Microfluid Nanofluid 10(6):1279–1288. doi:10.1007/s10404-010-0759-0

Noroozi Z, Kido H, Peytavi R, Nakajima-Sasaki R, Jasinskas A, Micic M, Felgner PL, Madou MJ (2011) A multiplexed immunoassay system based upon reciprocating centrifugal microfluidics. Rev Sci Instrum 82(6):064303. doi:10.1063/1.3597578

Ouyang Y, Wang S, Li J, Riehl PS, Begley M, Landers JP (2013) Rapid patterning of 'tunable' hydrophobic valves on disposable microchips by laser printer lithography. Lab Chip 13(9):1762–1771. doi:10.1039/c3lc41275j

Schembri CT, Burd TL, Kopf-Sill AR, Shea LR, Braynin B (1995) Centrifugation and capillarity integrated into a multiple analyte whole blood analyser. J Autom Chem 17(3):99–104

Schwemmer F, Zehnle S, Mark D, von Stetten F, Zengerle R, Paust N (2015) A microfluidic timer for timed valving and pumping in centrifugal microfluidics. Lab Chip 15:1545–1553. doi:10.1039/c4lc01269k

Siegrist J, Gorkin R, Clime L, Roy E, Peytavi R, Kido H, Bergeron M, Veres T, Madou M (2010) Serial siphon valving for centrifugal microfluidic platforms. Microfluid Nanofluid 9(1):55–63. doi:10.1007/s10404-009-0523-5

Steigert J, Brenner T, Grumann M, Riegger L, Lutz S, Zengerle R, Ducrée J (2007) Integrated siphon-based metering and sedimentation of whole blood on a hydrophilic lab-on-a-disk. Biomed Microdevices 9(5):675–679. doi:10.1007/s10544-007-9076-0

Strohmeier O, Keller M, Schwemmer F, Zehnle S, Mark D, von Stetten F, Zengerle R, Paust N (2015) Centrifugal microfluidic platforms: advanced unit operations and applications. Chem Soc Rev. doi:10.1039/c4cs00371c

Ukita Y, Ishizawa M, Takamura Y, Utsumi Y (2012) Internally triggered multistep flow sequencers using clepsydra. In: 16th international conference on miniaturized systems for chemistry and life sciences, pp 1465–1467

van Oordt T, Barb Y, Smetana J, Zengerle R, von Stetten F (2013) Miniature stick-packaging–an industrial technology for pre-storage and release of reagents in lab-on-a-chip systems. Lab Chip 13(15):2888–2892. doi:10.1039/c3lc50404b

Vázquez M (2011) Centrifugally-driven sample extraction, preconcentration and purification in microfluidic compact discs. Trends Anal Chem 30(10):1575–1586

Zehnle S, Schwemmer F, Roth G, von Stetten F, Zengerle R, Paust N (2012a) Centrifugo-dynamic inward pumping of liquids on a centrifugal microfluidic platform. Lab Chip 12(24):5142–5145. doi:10.1039/c2lc40942a

Zehnle S, Rombach M, von Stetten F, Zengerle R, Paust N (2012b) Microfluidic centrifugo-pneumatic siphon enables fast blood plasma extraction with high yield and purity. In: 16th international conference on miniaturized systems for chemistry and life sciences, pp 869–871

Zhao Y, Schwemmer F, Zehnle S, von Stetten F, Zengerle R, Paust N (2015) Centrifugo-pneumatic sedimentation, resuspension and transport of microparticles. Lab Chip 15:4133–4137. doi:10.1039/c5lc00508f